Nanoscale

COMMUNICATION

View Article Online
View Journal | View Issue

Published on 05 February 2015. Downloaded by North Carolina State University on 27/02/2015 16:03:34.

Cite this: *Nanoscale*, 2015, **7**, 4406

Received 18th November 2014,
Accepted 3rd February 2015

DOI: 10.1039/c4nr06840h

www.rsc.org/nanoscale

Fabrication of three-dimensional hierarchical nanostructures using template-directed colloidal assembly†

J. E. Elek, X. A. Zhang, B. Dai, Z. Xu and C.-H. Chang*

Optical effects in template-directed colloidal assembly are explored to fabricate microscale patterns with integrated three-dimensional (3D) nanostructures. This method allows the patterning of periodic nanostructures in arbitrarily designed regions by controlling particle assembly and light illumination. Using both "bottom-up" and "top-down" methods, this approach enables low-cost fabrication of hierarchical devices.

Much research interest has been drawn to the design and fabrication of ordered porous three-dimensional (3D) nanostructures. Surfaces utilizing periodic nanostructures have exhibited favorable properties such as enhanced surface wettability,[1–9] photonic structures,[9–14] and phononic properties.[15,16] Going beyond interesting material properties, such 3D porous materials can also be integrated into micro and macro devices, creating a hierarchical system and improving properties. The value of hierarchical nanostructured materials has been observed often in nature, such as improving superhydrophobicity in textured surfaces.[8] The nanoscale cilia atop the microscale pads of the gecko's foot enable conformal contact with surfaces of varying roughness for dry adhesion while scaling vertical surfaces.[17–19] Nano and microscale hierarchies on the leaf of the *Cotula fallax* provide unique moisture harvesting capabilities for nourishment.[3] Similarly, some species such as the *Stenocara gracilipes* beetle utilize alternating hydrophilic and hydrophobic microchannels on the wing to harvest moisture in the arid Namib Desert environment.[4–7] These natural phenomena have provided the inspiration, and many groups have fabricated similar engineered hierarchical structures for moisture harvesting.[5–7] In devices, micro batteries with 3D nanostructured electrodes have demonstrated large power densities rivalling many conventional supercapacitors.[20]

The fabrication of such hierarchical systems with 3D porous nanostructures is challenging due to their complex geometries at multiple lengthscales, and most existing techniques have limitations on scalability and precision. Direct laser writing using two-photon polymerization[21] has been used to demonstrate the fabrication of arbitrary nanostructures and can be used to pattern photonic circuits.[22] However this process is serial and can be difficult to scale. Interference or holographic lithography[9,15] can result in complex periodic 3D structures, however introducing phase-aligned microscale hierarchical structure is challenging. Self-assembly of colloidal particles[23–30] is a low-cost "bottom-up" approach, but can result in defects for 3D assembly.[29,30] Therefore, the development of a scalable fabrication process through which nano and microscale features can be independently controlled can further these research efforts in hierarchical structures.

In this work, we demonstrate the fabrication of hierarchical 3D nanostructures using illumination of organized patches of colloidal particles obtained using template-directed self-assembly (TDSA). In this approach, monodispersed spherical particles are guided by pre-determined topography to form microscale assemblies of colloidal crystals,[31–33] which can then be illuminated to create a 3D intensity pattern to selectively pattern the assembled regions. The resulting structures resemble a microscale organized channel consisting of porous periodic 3D nanostructures, thereby generating hierarchical architecture. The introduction of optical effects essentially takes TDSA to the third dimension, where the 3D nanostructure geometry is controlled by the particle parameters as governed by the Talbot effect.[34–38] The microscale organization of the assembly is determined by the template, which can be arbitrarily designed. The proposed method allows for the independent control of the micro and nanoscale features in hierarchical structures through the design of particle-light interactions and template parameters. This process enables the 3D nanostructures to be directed and spatial-phase aligned to the microscale template, which is achieved passively through the TDSA process. The process is also extremely low-cost, and is based on inexpensive and widely available

Department of Mechanical and Aerospace Engineering, North Carolina State University, Raleigh, North Carolina 27695, USA. E-mail: chichang@ncsu.edu

†Electronic supplementary information (ESI) available. See DOI: 10.1039/c4nr06840h

This journal is © The Royal Society of Chemistry 2015

Published on 05 February 2015. Downloaded by North Carolina State University on 27/02/2015 16:03:34.

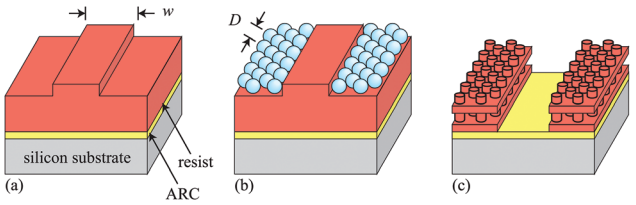

Fig. 1 Schematic of fabrication process. (a) Soft lithography is used to generate a surface-relief microstructured template in unexposed photoresist, which can be used to (b) direct and guide the assembly of colloidal particles. (c) Upon illumination, the regions under the assembled particles remain with 3D nanostructures.

materials and well-characterized processes. The process also eliminates the need for expensive masks often used in photolithography by replacing them with the colloidal lenses, minimizing the overall cost of the large-scale fabrication process. The lithography process also does not depend on light coherence, eliminating the need for expensive lasers and further reducing hardware requirements. The interactions of light and colloidal particles have been demonstrated as an attractive method for 3D nanolithography,[38,39] and here we extend the concept to pattern hierarchical structures.

The proposed method of 3D nanolithography using TDSA is characterized by three distinct processes, as illustrated in Fig. 1. First, the physical template is defined using solvent-assisted soft lithography[40,41] to produce a surface-relief topography on unexposed photoresist, as shown in Fig. 1(a). The master PDMS mold is patterned using standard microlithography processes, and can be defined to have arbitrary geometry. The solvent anneal process is performed at 95 °C, and the relatively low temperature process ensures the resist maintains photosensitivity. Colloidal particles can then be assembled within the recess regions in the photoresist template using convective assembly,[23–25] producing a template-directed monolayer of hexagonal close-packed colloids, as shown in Fig. 2(b). The substrate can then be illuminated at normal incidence to generate a 3D intensity pattern in the regions with assembled particles, which is recorded by the underlying photoresist. Upon development the resulting structures consist of microscale regions consisting of 3D nanostructures, as illustrated in Fig. 1(c). The nanostructure parameters can be controlled by the particle and illumination parameters, while the larger microstructure can be designed during soft lithography.

The fabricated photoresist template with surface-relief structures prepared using soft lithography is shown in Fig. 2(a). The template consists of a grating channel structure periodic in one direction, with raised ridge width of 1 μm and a trench width of 4 μm (for fabrication details see ESI A†). The depth of the template is controlled by the soft lithography template, and can be controlled from 100 to 500 nm. The template geometries are defined by the master pattern during the soft lithography process. Polystyrene nanospheres with 500 nm diameter are then assembled on the resist template using convective assembly, resulting in template-directed assembly. Cross-section and top-view scanning electron microscope (SEM) images of the template-directed colloidal assembly are seen in Fig. 2(b) and (c), respectively. The colloidal assembly is guided by the template direction as noted, and few point defects and grain boundaries are observed. Due to the rounded edges of the template topography, the number of particles within a single channel can be controlled, as described in more details in ESI B.†

Numerical simulation of the 3D lithography process using finite-difference time-domain (FDTD) methods[42] was conducted to predict the fabricated hierarchical structure, as illustrated in Fig. 3.

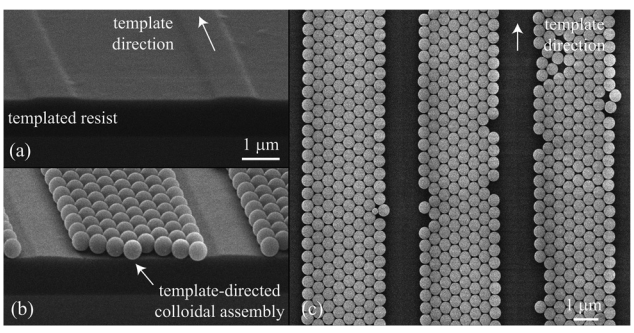

Fig. 2 (a) Unexposed photoresist template with width of 4 μm and depth of 200 nm. (b) Colloidal particles in hexagonal array aligned by the microscale template after convective assembly. (c) Top view of colloidal assembly within template regions.

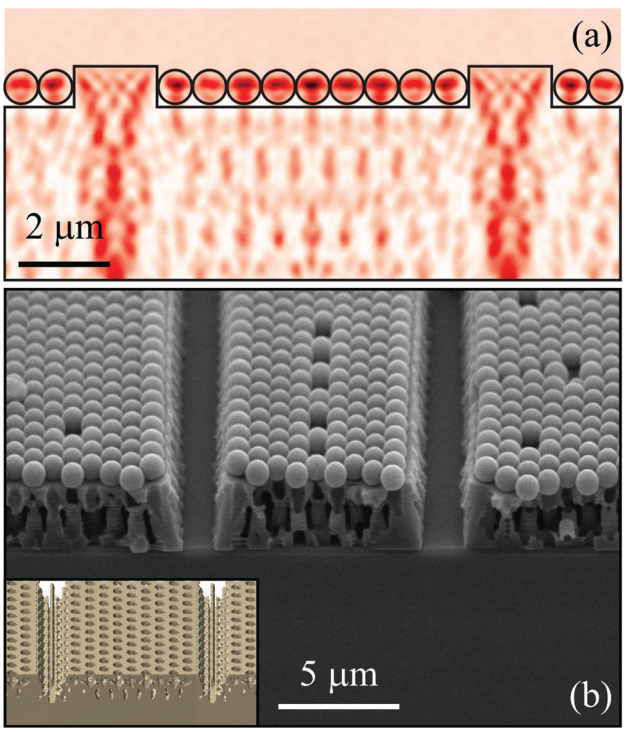

Fig. 3 (a) FDTD simulation of light intensity under the illuminated template-directed colloidal assembly. (b) Cross-sectional micrograph of fabricated hierarchical 3D nanostructure with nanospheres. The predicted geometry using FDTD and binary resist model can be seen in the inset diagram.

Published on 05 February 2015. Downloaded by North Carolina State University on 27/02/2015 16:03:34.

The model simulates the intensity pattern within a unit cell of the microscale template, and assumes periodic boundary conditions in x and y directions. Perfectly match layers were used for the upper and lower sides in z direction to apply absorbing boundary conditions. Light with 365 nm wavelength propagates through the colloidal nanoparticles and diffracts into the photoresist, resulting in a periodic intensity under the particles. Intensity pattern using both transverse electric (TE) and transverse magnetic (TM) polarized light were simulated, and the non-polarized intensity contour is calculated by the average and depicted in Fig. 3(a). The SEM images of the fabricated structure using the simulated conditions are illustrated in Fig. 3(b). The colloids were not removed prior to development in this sample for a direct comparison with the simulation results, and can be seen still assembled on the final structures. The effect of the assembled particles on the underlying structures can be directly observed in the experimental results, which resulted in periodic 3D nanostructures in assembled regions. Edge diffraction effects can be observed for the regions without the colloidal particles, which results in complete photoresist exposure as shown in the fabricated structures. The FDTD model can be combined with a binary resist model to predict the resulting photoresist structure,[38,39] as shown in the inset image, and agrees well with the fabricated structures.

The patterned 3D nanostructures are governed by the Talbot effect, and can be controlled by the incident light wavelength and the particle diameters. The axial period of the structure is described by the Talbot distance:[35,38]

$$z_t = \frac{\lambda/n}{1 - \sqrt{1 - (\lambda/n\Lambda)^2}}$$

where λ is incident light wavelength, n is the photoresist refractive index, and Λ is the lateral period of the particle assembly. For a hexagonal array of spherical particles with diameter D, the periodicity can be defined as $\Lambda = D\sqrt{3}/2$. Therefore, the lattice parameters of the 3D nanostructure can be controlled by varying particle size and exposure wavelength. Note the design of the nanostructure is independent of the microscale template features.

To examine the design of the nanostructure lattice parameters of the hierarchical 3D structures, various particle diameters and wavelength exposure configurations were used in conjunction with the 1D microscale template with ridge width of 1 μm and trench width of 4 μm. In this experiment, particles with D = 350, 390, and 500 nm were each exposed to UV light with wavelength λ = 325, 365, and 405 nm. Coherence is not required for lithography, and the light source for the two longer wavelengths is a bandpass filtered mercury lamp. The fabricated 3D hierarchical structures are illustrated in Fig. 4 (additional results are shown in the ESI C†).

Fig. 4(a) and (b) depict the top-view and cross-section micrographs, respectively, for the structures fabricated using D = 500 nm and λ = 325 nm, resulting in measured axial period z_t = 1790 nm. The direction of the template is denoted by the arrow, and guides the alignment of the patterned 3D nanostructures, as observed in Fig. 4(b). The porous nanostructures make up the larger microstructure channel, which has a width of 4 μm and is defined by the original template. The ripple effect observed on the sidewall is due to reflection of the UV light from the silicon substrate, and can be suppressed using antireflective coating.

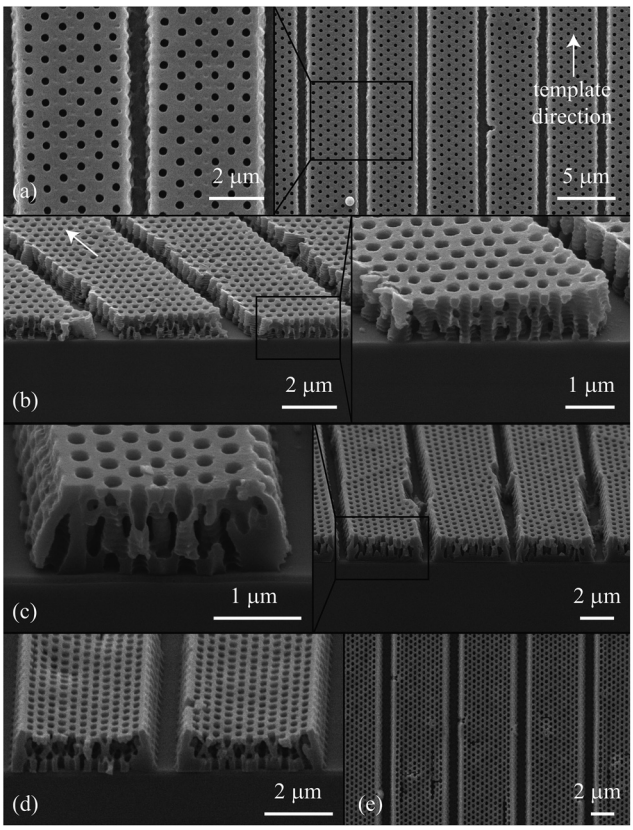

Fig. 4 Fabrication results of micro channels consisting of 3D nanofabrication. (a) Top-view and (b) cross-section micrographs for D = 500 nm and λ = 325 nm exposure. (c) Cross-section micrographs for D = 500 nm and λ = 365 nm. (d) Cross-section and (e) top-view micrographs of D = 390 nm and λ = 325 nm.

The structures shown in Fig. 4(c) are fabricated using D = 500 nm and λ = 365 nm, resulting in a shorter axial period z_t = 1497 nm. These result indicate that various lattice parameters can be patterned using a single particle diameter by illuminating with different wavelength light to control the Talbot effect. Fig. 4(d) and (e) depict cross-section and top-view micrographs, respectively, of the structure fabricated using D = 390 nm and λ = 325 nm, which has a measured z_t = 1057 nm. This result also indicates that the same wavelength exposure coupled with different particle diameters can also result in different lattice parameters. Note for all of the fabricated structures the larger microstructure is defined by the same template and maintains a constant width of 4 μm. These results demonstrate that the nanostructure lattice parameters and the larger microstructure can be independently controlled. The use of larger template geometries would increase the microstructure width but not the nanostructure, as shown in ESI D.†

 This journal is © The Royal Society of Chemistry 2015

Published on 05 February 2015. Downloaded by North Carolina State University on 27/02/2015 16:03:34.

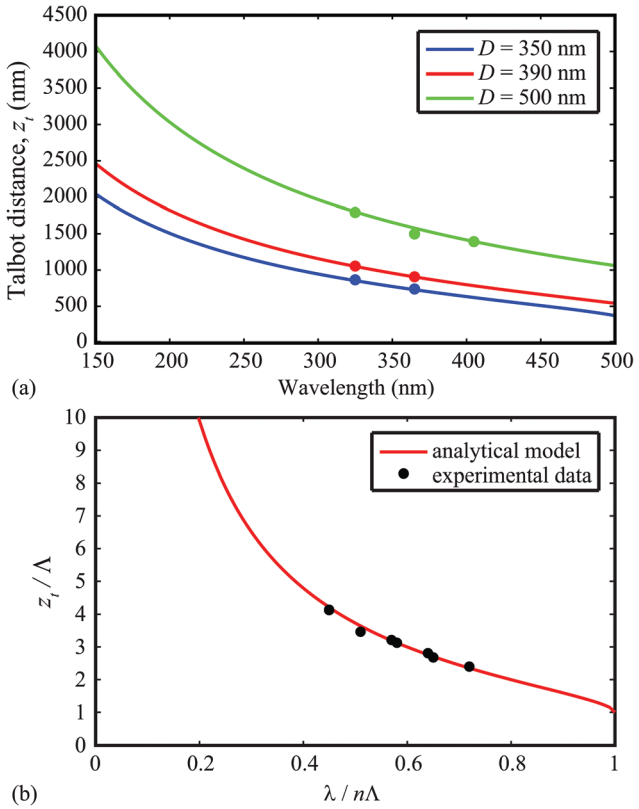

Fig. 5 Theoretical and measured data for (a) lateral period *vs.* exposure wavelength and (b) normalized period *vs.* γ.

The measured axial period of the fabricated structures can be compared with the theoretical Talbot distances for each particle size and exposure wavelength combination. Fig. 5(a) plots the theoretical axial period as a function of exposure wavelength with the experimental data for particle diameters of 500, 390, and 350 nm (for detailed data see ESI C†).

The model and data agree well, indicating that the axial period is scaled by the particle diameter and can be designed over a finite range by selecting the exposure wavelength. The particle diameter effect can be removed by normalizing the axial period and wavelength by the lateral period to better examine the scaling relationships. Fig. 5(b) illustrates the theoretical and experimental normalized axial period, z_t/Λ, as a function of the dimensionless wavelength parameter $\gamma = \lambda/n\Lambda$. The data from different particle diameters and exposure wavelengths agree well with the theoretical model, which exhibits an inverse relationship between the structure axial period and exposure wavelength. The measurement uncertainty and error for the data points ranged up to 5%, demonstrating a high level of control over the nanostructure lattice parameters.

The colloidal particle sizes used for the experiments were chosen to have similar sizes to the exposure wavelength; however there is no theoretical constraint on particle sizes. The Talbot effect scales readily, and much larger or smaller structures can be fabricated using longer and shorter wavelength, respectively. In addition, the pattern and the template geometry can be arbitrarily chosen to control the larger microscale structure, and is the subject of future studies. Therefore, the many combinations of particle, light, and template parameters can be controlled to achieve precise control of the nanoscale and microscale features.

In this work, we demonstrated a low-cost technique for fabricating complex hierarchical 3D micro and nanostructures using both "top-down" and "bottom-up" methods. This process enables the patterning of 3D nanostructure in specifically designed regions through TDSA of colloidal particles. This approach allows for control of the microscale through template designing, while maintaining the ability to independently control the nanoscale features through specifying the particle sizes and exposure wavelength. The key mechanism of generating complex 3D structures using light interactions with template-directed colloidal arrays is scalable, low-cost, and does not require extensive hardware. While the present work focuses on polymer structures, other materials may be introduced by using conformal depositions techniques such as atomic layer deposition. The demonstrated hierarchical 3D structures can find potential applications in photonic circuits, micro/nanofluidics, and moisture harvesting devices.

The authors thank Goran Rasic for helpful discussions, and the students, staff, and facility from the Nanofabrication Facility (NNF) and the Analytical Instrumentation Facility (AIF) at North Carolina State University. This work was supported by a NASA Office of the Chief Technologist's Space Technology Research Opportunity – Early Career Faculty grant (grant NNX12AQ46G) and by the Ralph E. Powe Junior Enhancement Award from the Oak Ridge Associated Universities (ORAU).

Notes and references

1 A. Lafuma and D. Quéré, *Nat. Mater.*, 2003, **2**, 457–460.
2 E. Martines, K. Seunarine, H. Morgan, N. Gadegaard, C. D. W. Wilkinson and M. O. Riehle, *Nano Lett.*, 2005, **5**(10), 2097–2103.
3 H. G. Andrews, E. A. Eccles, W. C. E. Schofield and J. P. S. Badyal, *Langmuir*, 2011, **27**, 3798–3802.
4 A. R. Parker and C. R. Lawrence, *Nature*, 2001, **414**, 33–34.
5 R. P. Garrod, L. G. Harris, W. C. E. Schofield, J. McGettrick, L. J. Ward, D. O. H. Teare and J. P. S. Badyal, *Langmuir*, 2007, **23**, 689–693.
6 C. Dorrer and J. Ruhe, *Langmuir*, 2008, **24**, 6154–6158.
7 L. Zhai, M. C. Berg, F. C. Cebeci, Y. Kim, J. M. Wilwid, M. F. Rubner and R. E. Cohen, *Nano Lett.*, 2006, **6**(6), 1213–1217.
8 D. J. Lee, H. M. Kim, Y. S. Song and J. R. Youn, *ACS Nano*, 2012, **6**(9), 7656–7664.
9 K.-C. Park, H. J. Choi, C.-H. Chang, R. E. Cohen, G. H. McKinley and G. Barbastathis, *ACS Nano*, 2012, **6**(5), 3789–3799.
10 S. Y. Lin, J. G. Fleming, D. L. Hetherington, B. K. Smith, R. Biswas, K. M. Ho, M. M. Sigalas, W. Zubrycki, S. R. Kurtz and J. Bur, *Nature*, 1998, **394**, 251–253.

Published on 05 February 2015. Downloaded by North Carolina State University on 27/02/2015 16:03:34.

11 S. Noda, K. Tomoda, N. Yamamoto and A. Chutinan, *Science*, 2000, **289**(5479), 604–606.
12 M. Qi, E. Lidorikis, P. T. Rakich, S. G. Johnson, J. D. Joannopoulos, E. P. Ippen and H. I. Smith, *Nature*, 2004, **429**, 538–542.
13 P. Vukusic and J. R. Sambles, *Nature*, 2003, **424**, 852–855.
14 J. Hiller, J. D. Mendelsohn and M. F. Rubner, *Nat. Mater.*, 2002, **1**, 59–63.
15 J.-H. Jang, C. K. Ullal, T. Gorishnyy, V. V. Tsukruk and E. L. Thomas, *Nano Lett.*, 2006, **6**(4), 740–743.
16 V. Jean, S. Fumeron, K. Termentzidis, S. Tutashkonko and D. Lacroix, *J. Appl. Phys.*, 2014, **115**, 024304.
17 K. Autumn, M. Sitti, Y. A. Liang, A. M. Peattie, W. R. Hansen, S. Sponberg, T. W. Kenny, R. Fearing, J. N. Israelachvili and R. J. Full, *Proc. Natl. Acad. Sci. U. S. A.*, 2002, **99**(19), 12252–12256.
18 J. Yu, S. Chary, S. Das, J. Tamelier, N. S. Pesika, K. L. Turner and J. N. Israelachvili, *Adv. Funct. Mater.*, 2011, **21**(16), 3010–3018.
19 B. Bhushan, *J. Adhes. Sci. Technol.*, 2007, **21**(12–13), 1213–1258.
20 J. H. Pikul, J. C. Zhang, P. V. Braun and W. P. King, *Nat. Commun.*, 2013, **4**, 41732.
21 S. Maruo, O. Nakamura and S. Kawata, *Opt. Lett.*, 1997, **22**, 132–134.
22 M. Deubel, M. Wegener, S. Linden, G. von Freymann and S. John, *Opt. Lett.*, 2006, **31**(6), 805–807.
23 L. Malaquin, T. Kraus, H. Schmid, E. Delamarche and H. Wolf, *Langmuir*, 2007, **23**, 11513–11521.
24 B. G. Prevo, J. C. Fuller and O. D. Velev, *Chem. Mater.*, 2005, **17**, 28–35.
25 O. D. Velev and S. Gupta, *Adv. Mater.*, 2009, **21**, 1897–1905.
26 Z. Dai, L. Jia, G. Duan, Y. Li, H. Zhang, J. Wang, J. Hu and W. Cai, *Chem. – Eur. J.*, 2013, **19**(40), 13387–13395.
27 Y. Li, G. Duan, G. Liu and W. Cai, *Chem. Soc. Rev.*, 2013, **42**(8), 3614–3627.
28 X. Li, Y. Wu, L. Hang, D. Men, W. Cai and Y. Li, *J. Mater. Chem. C*, 2014, **3**(1), 51–57.
29 O. D. Velev and E. W. Kaler, *Adv. Mater.*, 2000, **12**, 531–534.
30 B. Gates, D. Qin and Y. Xia, *Adv. Mater.*, 1999, **11**(6), 466–469.
31 A. van Blaaderen, R. Rue and P. Wiltzius, *Nature*, 1997, **385**, 321–324.
32 Y. Xia, Y. Yin, Y. Lu and J. McLellan, *Adv. Funct. Mater.*, 2003, **13**(12), 907–918.
33 M. Rycenga, P. H. C. Camargo and Y. Xia, *Soft Matter*, 2009, **5**, 1129–1136.
34 H. F. Talbot, *Philos. Mag. Series 3*, 1836, **9**(56), 401–407.
35 L. Rayleigh, *Philos. Mag. Series 5*, 1881, **11**(67), 196–205.
36 S. Jeon, J.-U. Park, R. Cirelli, S. Yang, C. E. Heitzman, P. V. Braun, P. J. A. Kenis and J. A. Rogers, *Proc. Natl. Acad. Sci. U. S. A.*, 2004, **101**, 12428–12433.
37 J.-H. Jang, C. K. Ullal, M. Maldovan, T. Gorishnyy, S. Kooi, C. Koh and E. L. Thomas, *Adv. Funct. Mater.*, 2007, **17**, 3027–3041.
38 C.-H. Chang, L. Tian, W. Hesse, H. Gao, H. J. Choi, J.-G. Kim, M. Siddiqui and G. Barbastathis, *Nano Lett.*, 2011, **11**, 2533–2537.
39 X. A. Zhang, J. Elek and C.-H. Chang, *ACS Nano*, 2013, **7**(7), 6212–6218.
40 E. King, Y. Xia, X.-M. Zhao and G. M. Whitesides, *Adv. Mater.*, 1997, **9**(8), 651–654.
41 Y. Xia and G. M. Whitesides, *Annu. Rev. Mater. Sci.*, 1998, **28**, 153–184.
42 A. F. Oskooi, D. Roundy, M. Ibanescu, P. Bermel, J. Joannopoulos and S. G. Johnson, *Comput. Phys. Commun.*, 2010, **181**, 687–702.

 This journal is © The Royal Society of Chemistry 2015